RSC Advances

PAPER

View Article Online
View Journal | View Issue

Cite this: *RSC Adv.*, 2018, **8**, 25159

Bicontinuous and cellular structure design of PVDF membranes by using binary solvents for the membrane distillation process†

Ziyi Wang,[ad] Yuanyuan Tang *[a] and Baoan Li *[bc]

With excellent permeability as the foremost requirement for membranes used in the membrane distillation (MD) process, the thermally induced phase separation (TIPS) method is a promising approach for preparing porous membranes with a bicontinuous structure, which is identified as the best morphology for permeation. The structure design of membranes prepared by the TIPS process can be strengthened when a binary solvent is introduced in the casting solution. In this work, the determination principles for binary solvent were explicated in detail, and further employed for the selection of binary solvent for the fabrication of polyvinylidene fluoride (PVDF) membrane with different structures. By the TIPS approach, the porous PVDF hollow fiber membranes with cellular structure were generated by g-butyrolactone (GBL)/dioctyl phthalate (DOP) and GBL/dioctyl adipate (DOA) binary solvents, while the membrane with a bicontinuous structure was produced from GBL/dioctyl sebacate (DOS) binary solvent. The phase diagram was used to explain a feasible mechanism for the formation of the porous structures above. When the morphologies and properties of the membranes were characterized and compared, the membrane with a bicontinuous structure rather than a cellular structure was identified as the potential structure for MD processes with much higher tensile strength, narrower pore size distribution, higher MD flux and excellent long-term performance.

Received 28th March 2018
Accepted 2nd July 2018

DOI: 10.1039/c8ra02692k

rsc.li/rsc-advances

1. Introduction

The membrane distillation (MD)[1] technique is a kind of membrane separation technology combined with traditional distillation technology, which has been widely used in chemical separation and enrichment,[2] seawater desalination[3] and industrial waste water treatment.[4] Among the membrane materials applied in the MD process, semi-crystalline polyvinylidene fluoride (PVDF) has attracted much attention owing to its notable chemical stability, stain resistance, mechanical properties, wide processing temperature, and pliability.[5–7] Nonsolvent induced phase separation (NIPS), which is usually considered as a common strategy for preparing PVDF membranes,[8] induced the formation of macrovoid and finger-like structures inside the membrane due to the exchange of solvent for a non-solvent phase. The defects caused by the NIPS process resulted in unsatisfactory mechanical properties, which are detrimental to long-term practical application especially at high temperature. The thermally induced phase separation (TIPS) method,[9] by contrast, is a promising approach for preparing porous membranes due to several accepted advantages, such as fewer influencing factors, easy operation, uniform pore size distribution, high porosity, excellent mechanical properties and so on.

In the TIPS process, the homogeneous casting solution is obtained by dissolving the polymer in the solvent with high boiling point and low molecular weight at an elevated temperature. Then the casting solution is shaped into a flat sheet or hollow fiber and cooled in the coagulation bath to induce phase separation and solidify the membrane. Finally, the residual solvent is extracted by extractant which is further evaporated to yield the porous structure. As the thermal energy is removed from the homogeneous solution, TIPS occurs in the form of solid–liquid (S–L) or liquid–liquid (L–L) phase separation.[7] The final morphology of the membrane is strongly influenced by the sequence of L–L and S–L phase separation. When the L–L phase separation is prior to S–L phase separation, the membrane morphology is always characterized as cellular or bicontinuous structures with excellent connectivity and high porosity. However, unexpected spherulitic structures can also be formed

[a]*School of Environmental Science and Engineering, Southern University of Science and Technology, 1088 Xueyuan Blvd, Nanshan District, Shenzhen 518055, P. R. China. E-mail: tangyy@sustc.edu.cn*

[b]*Chemical Engineering Research Center, School of Chemical Engineering and Technology, Tianjin University, Tianjin 300354, China*

[c]*Collaborative Innovation Center of Chemical Science and Engineering, Tianjin 300354, China*

[d]*School of Chemical Engineering and Technology, Nankai University, Tianjin 300072, China*

† Electronic supplementary information (ESI) available: Calculation of porosity and pore size distribution, figures of membrane fabrication and property measurements, phase diagram analysis. See DOI: 10.1039/c8ra02692k

when the S–L phase separation occurs first, which exhibits poor membrane strength, a dense skin layer and wide pore size distribution due to the strong interaction between the PVDF material and diluents. The compatibility of the system has been reported as the main factor determining whether L–L or S–L phase separation occurs.[8] Compared with the single diluent system, the structure design can be strengthened when a binary diluent is introduced in the casting solution. Tang *et al.* introduced a binary solvent of diphenyl ketone (DPK) and 1,2-propylene glycol (PG) to control the mechanisms of the phase separation, and the bicontinuous cross-section structure was obtained when the PG/DPK mass ratio is 3/7 and the polymer concentration is 30 wt%.[9] Zhou *et al.* employed a binary solvent of dibutyl phthalate/dioctyl phthalate (DBP/DOP) to prepare PVDF hollow fiber membranes *via* a TIPS process, and found that the membrane morphology changed from spherulite structure to uniform interconnected sponge-like structure when the weight ratio DBP to DOP was changed.[10] Song *et al.* used a binary solvent consisting of DBP and dibutyl sebacate (DBS) to fabricate PVDF membranes, and found that the morphology of the membrane cross-section changed from spherulitic to bicontinuous structure as the DBS mass fraction increased in the mixed solvent.[8]

In contrast with macrovoid, finger-like, sponge-like and spherulitic structures, the cellular and bicontinuous structures are identified as beneficial structures in MD process due to their excellent permeability.[11] A plenty of works have been done on the fabrication of PVDF hollow fibre membranes with the cellular and bicontinuous structures for the purpose of membrane distillation.[12] However, the selection of binary solvent has not yet been deeply explicated for preparing the membranes with the cellular structure and bicontinuous structure. Moreover, seldom information was reported currently for an extensive comparison between these two structures. In this work, the determination principles of binary solvent for TIPS process were summarized in detail. The feasible binary solvent was employed to generate the porous PVDF hollow fiber membranes with the cellular structure and bicontinuous structure by TIPS approach. The phase diagram was used for analyzing the possible formation mechanisms of different structures. The morphology, property and operation performance in direct contact membrane distillation (DCMD) of the hollow fiber membranes were characterized and compared. On the basis of our findings and comparison with the other MD membranes in references, this study schematically proposed a promising strategy to design PVDF membrane with the cellular structure and bicontinuous structure, and improved the performance of PVDF membrane in MD process.

2. Materials and methods

2.1. Binary diluent determination

The determination principles of solvent employed in TIPS process should comply with the following schemes: (1) the principles for solvent determination varied with polymer categories.[13] As a polar semi-crystalline polymer, the rules of "like dissolves like" and "solubility parameters theory" are supposed to be followed by PVDF for the solvent determination. That means, PVDF can be soluble in a polar solvent or a solvent with similar solubility parameter. (2) A homogeneous solution is formed at an elevated temperature by blending the polymer with a high-boiling, low molecular weight solvent. The initial temperature must be less than the boiling point of solvent and is typically 25 to 100 °C greater than the melting temperature or glass transition temperature of pure polymer. The polymer must be stable and the solvent should have low volatility at this temperature. For PVDF, the melting point of which is about 160–170 °C, the solvent with boiling point more than 200 °C is desirable for preventing severely volatilization. (3) The solution is supposed to be fabricated into the desired shape (flat sheet, tube, or hollow fiber) only at appropriate viscosity.[14] Thereby the low fluidity and mobility of solvent are detrimental to the membrane fabrication. (4) Low toxicity and low corrosivity are preferred. (5) Low price commercial products are favorable to control the production cost.

Following the disciplines outlined above, we have selected four solvents for PVDF membrane fabrication by TIPS method, the parameters of which were listed in Table 1. In order to verify the compatibility between PVDF and each solvent, PVDF powder (Solef 6008, $M_w = 2.55 \times 105$, $M_w/M_n = 1.9$, m.p. 174 °C, Solvay Solexis) was mixed with GBL, DOP, DOA and DOS with a mass ratio of PVDF : solvent = 7 : 3 at 200 °C respectively to form four suspensions. GBL, DOP, DOA and DOS were analytical reagents (AR grade) and purchased from Guangfu Fine Chemical Research Institute (Tianjin, China). All chemicals used in this study were not purified further. For PVDF, a polar semi-crystalline polymer, polarity and solubility parameter should be both considered for the solvent determination. The high dielectric constant value of GBL (39) indicated its strong polarity. Though the great difference of solubility parameter between PVDF (19.2 $(J\ cm^{-3})^{1/2}$) and GBL (26.3 $(J\ cm^{-3})^{1/2}$), the polar PVDF can be dissolved in GBL at high temperature according to the "like dissolves like" principle. Conversely, even with the close solubility parameter (19.2 $(J\ cm^{-3})^{1/2}$ for PVDF, 18.2 $(J\ cm^{-3})^{1/2}$ for DOP, 17.4 $(J\ cm^{-3})^{1/2}$ for DOA and 17.2 $(J\ cm^{-3})^{1/2}$ for DOS), the big gap in dielectric constant between

Table 1 The parameters of four solvents[15] and the compatibility between PVDF and each solvent observed in this study

Materials	Boiling point (°C)	Solubility parameter $(J\ cm^{-3})^{1/2}$	Dielectric constant	Viscosity (mPa s)	Compatibility
GBL	204	26.3	39	1.7	Dissolved/strong
DOP	284	18.2	5.3	81.4	Swollen/weak
DOA	214	17.4	4–5	13.7	Swollen/weaker
DOS	377	17.2	<4	19.9	Undissolved/weakest

PVDF (8–9) and DOP (5.3), DOA (4–5) and DOS (<4) demonstrated a great difference in polarity. Therefore, the poor compatibility between PVDF and the other three solvents were characterized and listed in Table 1.

It is generally accepted that the single diluent casting solution is incapable of adjusting the polymer–diluent interaction. Based on the above theoretical considerations and experimental results, binary diluent is supposed to be essential for adjusting the compatibility between polymer and diluent. In the following experiment, therefore, the strong diluent GBL was mixed with the other three weak diluents (DOP, DOA and DOS) at the mass ration of GBL : weak diluent = 3 : 7 to form three binary diluents in different compatibility. Afterwards, PVDF was dispersed in each binary diluent at the weight percentage of 25 wt% to produce three homogeneous casting solutions. The membranes prepared from PVDF/GBL/DOP (casting solution a, CA), PVDF/GBL/DOA (casting solution b, CB), and PVDF/GBL/DOS (casting solution c, CC) are named as membrane a (MA), membrane b (MB), and membrane c (MC) respectively. The influence of binary diluent composition on the phase separation, membrane structure and performance was explored.

2.2. Fabrication of hollow fiber membranes

To gain a better understanding of binary solvent system, the as-prepared casting solutions were employed for the following fabrication process. An extrusion apparatus was used to fabricate hollow fiber membrane as shown in Fig. S1 of ESI.† The feasible casting solution was fed to the vessel, heated to 190 °C with stirring for 2 h under the nitrogen atmosphere. After releasing the air bubbles for 1 h, the homogeneous casting solution was fed to a spinneret under the nitrogen pressure of 0.2 MPa. The spinneret is consisted of an outer tube and an inner tube with diameters as 3.1 and 1.1 mm, respectively. Another stream of nitrogen was blown into the spinneret to make a lumen at the center of the fiber. The solution was partly cooled in the air, and then entered into the coagulation bath to induce the phase separation and solidify the membrane. The distance between spinneret and bath was 10 cm. The extrusion rate was fixed as 8 mL min^{-1}. The solidified hollow fiber membrane was collected by a take-up machine and further extracted by immersion in ethanol for 24 h to remove the residual solvent. At last, the wet membrane was dried in the air at room temperature until yielding porous membrane.

2.3. Membrane characterization

The hollow fiber membrane was freeze-fractured in liquid nitrogen to yield cross section. For better visualization of the morphology, the surface and cross section of the membrane were coated with gold (E1020, Hitachi), followed by observation using field emission scanning electron microscopy (SEM, S-4800, Hitachi). Due to the inherent elasticity and flexibility, the outer diameter, inner diameter and thickness were also measured by SEM instead of vernier caliper and screw micrometer. The phase identification of the hollow fiber membrane based on the XRD pattern was collected through an X-ray diffractometer (Rigaku Smartlab) equipped with Cu Kα (λ = 1.5405 Å) radiation source at 30 kV and 40 mA. The 2θ scanning range was operated in a transmission mode from 10 to 30° with a scanning speed of 10° min^{-1}. The overall porosity and pore size distribution of the membrane were determined by gravimetric method and bubble point method, respectively. The detailed description and calculation of porosity and pore size distribution were provided in Appendix 1 and Fig. S2 of the ESI.† The tensile strength of the hollow fiber membrane was measured using a universal testing machine (MZ-5000C, Jiangdu Mingzhu). The membrane was fixed vertically between two pairs of tweezers with the length of 10 cm. Then the membrane was extended at a constant elongation rate of 10 mm min^{-1} until it was broken. Every specimen was tested 10 times. The contact angle of each membrane was measured at room temperature by the sessile drop method *via* a contact angle instrument (Dataphysics OCA15EC, Germany). The adopted water droplet volume is 5 μL. For the measurement of contact angle, three replicates were randomly selected on the membrane surface.

DCMD test was carried out to evaluate the permeability of the fabricated hollow fiber membranes, the schematic diagram of which was shown in Fig. S3 of ESI.† Several PVDF hollow fiber membranes were assembled and encapsulated into a module. A hot NaCl solution with 3.5 wt% by mass concentration was reserved in a thermostatic tank as feed. The water vapor was evaporated from the feed side and transferred across the fiber into the permeation side. The permeated water vapor was condensed by a cooler and then flowed into the permeate stream collector through the lumen of the hollow fiber membranes with a magnetic pump. The permeate stream amount was measured and recorded by an electrical balance and a computer, respectively. The DCMD flux of the hollow fiber membranes was calculated based on the inner surface area of membranes by the following equation:

$$F = \frac{\Delta M}{\pi d l t n} \quad (1)$$

where F is the permeate flux (kg $(m^2\ h)^{-1}$), ΔM is the quantity of distillate (kg), d is the diameter of the fiber (m), l is the length of the fiber (m) and t is the system running time (h), n is the number of fibers.

The electric conductivity of the distillate was determined using an electric conductivity meter (RC-19, Beckman) at 25 °C to measure the salt rejection of the membrane. To further estimate the long-term performance of the membrane, the DCMD process was extended to 240 h at the feed inlet temperature of 70 °C. The flux of the membrane was recorded every 10 h in this continuously running process. Afterwards, the surface and cross section morphology of the membrane were observed by SEM testing again. Chemical cleaning has been undertaken to address the issue of membrane fouling. Chemical cleaning was performed by drawing some cleaning chemical into the lumen of the membrane and soaking the module in each of the cleaning agent for 12 h. The sequence of chemical cleaning was alkali treatment of the module, followed by a brief rinse of the module with DI water, and then acid treatment of the module. The alkali used is a mixture of 1 mol L^{-1} NaOH and

0.05% sodium hypochlorite solution while 1 mol L^{-1} HNO_3 solution was used for acid treatment. Then the surface and cross section of the cleaned membranes were coated with gold, followed by observation using SEM testing.

3. Results and discussion

3.1. Properties of hollow fiber membranes

In principle, the final membrane structure is thought to rely on the thermodynamic state of the casting solution to be quenched, as schematized by the phase diagram of Fig. S4 in ESI.† Fig. 1 exhibits the surface and cross section morphology of MA, MB and MC. A skin layer can be observed in each membrane surface as demonstrated in Fig. 1a–c. The quick evaporation of casting solution extruded from the spinneret (above 180 °C) induced great concentration difference between the surface and internal of the membrane.[16] The subsequent solvent diffusion from membrane surface to water also caused the increase of polymer concentration at the surface[17] when the membranes were solidified in cooling bath. The formation of skin layer was determined by the entire solidification process, and showed no indication of morphology variation with the casting solution. This skin layer served as a barrier for providing high selectivity in MD process.

The different binary solvents used in this study were taken to be indicative for engineering of the membrane structures. The cellular structure in Fig. 1d and e and bicontinuous structure in Fig. 1f demonstrate that these three casting solutions in certain composition followed the right branch of the binodal curve as the phase diagram shown in Fig. S4b of ESI.† The casting solutions entered the region between the binodal and spinodal curves, and became the droplets dispersion of polymer-lean phase and polymer-rich phase. Under the driving force of surface energy difference at the interface of two phases, the droplets in the same phase merged together gradually, with eventual growth into larger ones. In CA and CB, the polymer-rich phase droplets grew into the solid spherulites while the merging of polymer-lean phase droplets until the casting solution reached the crystallization curve. The spherulites transformed into cell walls eventually, meanwhile the collision of growing polymer-lean phase droplets became the pores connecting the cells, finally forming the cellular structure. By comparison with CA, the bigger difference in dielectric constant between PVDF and DOA induced the worse compatibility of CB and thus the larger gap between binodal curve and crystallization curve. The longer coarsening time allowed greater growth of pores without qualitatively altering the structure, which can be clearly observed in Fig. 1e. In the same way, the biggest difference of dielectric constant between PVDF and DOS induced the worst compatibility of CC and the largest space between binodal curve and crystallization curve. The polymer-rich phase droplets in CC transferred into the spherulites with interconnected pores as temperature dropped down. The boundary among the polymer-lean phase droplets disappeared and gap junction pores were formed gradually during their collision. The connection of interconnected pores and gap junction pores constituted the bicontinuous structure (Fig. 1f) due to the longest coarsening time, which is identified as the best membrane structure with excellent permeability.

Fig. 1g–i reveals no morphology variation, the macrovoid structures could be observed in the inner surface of each membrane. The inner surface was exposed to the nitrogen which was already heated by the surrounding solution, inducing a long time for cooling the casting solution to the coagulation bath temperature, as well as barely evaporation of solvents at the inner surface. The enough time for the collision and growth of the droplets was beneficial for the generation of macrovoid.

Besides, the high solvent content at the inner surface provided substantial space for pores growth when extraction

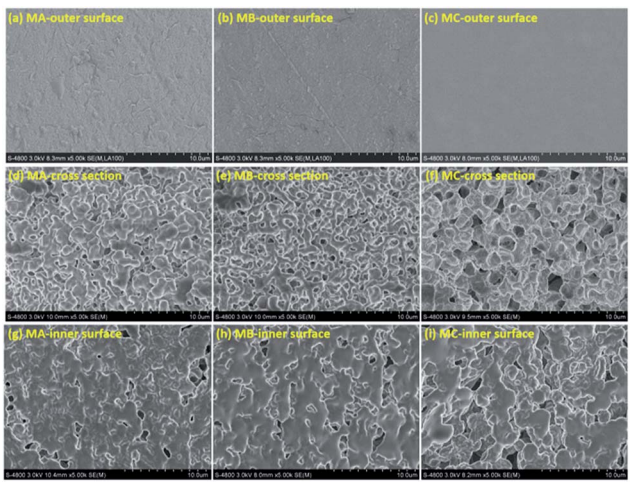

Fig. 1 The surface and cross section morphology of membrane a (MA), membrane b (MB) and membrane c (MC) prepared from PVDF/GBL/DOP (casting solution a, CA), PVDF/GBL/DOA (casting solution b, CB), and PVDF/GBL/DOS (casting solution c, CC), respectively.

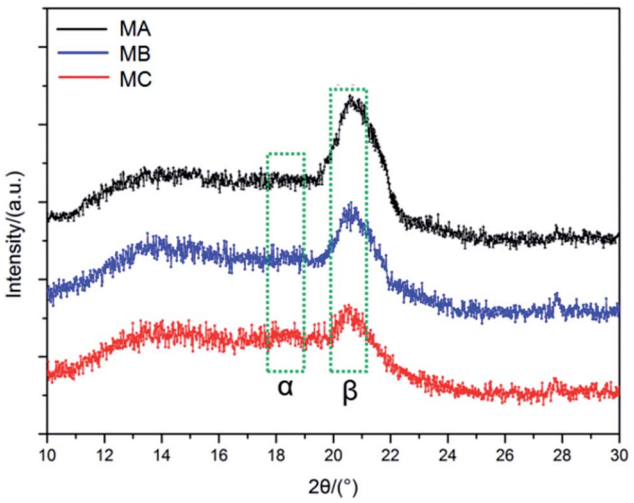

Fig. 2 The crystalline form of membrane a (MA), membrane b (MB) and membrane c (MC) prepared from PVDF/GBL/DOP (casting solution a, CA), PVDF/GBL/DOA (casting solution b, CB), and PVDF/GBL/DOS (casting solution c, CC), respectively.

Table 2 Several characteristics of membrane a (MA), membrane b (MB) and membrane c (MC) prepared from PVDF/GBL/DOP (casting solution a, CA), PVDF/GBL/DOA (casting solution b, CB), and PVDF/GBL/DOS (casting solution c, CC), respectively

Code	Outer diameter (mm)	Inner diameter (mm)	Thickness (μm)	Porosity (%)	Mean pore size (μm)	Tensile strength (MPa)	Elongation (%)	Contact angle (°)
MA	1.06 ± 0.05	0.71 ± 0.08	175 ± 17	56.7 ± 1.5	0.29 ± 0.01	4.74 ± 0.16	51.06 ± 0.34	109.3 ± 1.2
MB	1.07 ± 0.04	0.72 ± 0.05	175 ± 12	63.9 ± 1.7	0.30 ± 0.02	5.32 ± 0.23	55.37 ± 0.31	111.4 ± 0.8
MC	1.09 ± 0.02	0.75 ± 0.06	170 ± 20	67.2 ± 2.0	0.32 ± 0.02	6.59 ± 0.19	62.66 ± 0.29	107.8 ± 1.5

occurred, which also leaded to the increase of pore size. In this regard, the macrovoid can be formed at the inner surfaces of three membranes even with different phase separation mechanisms.

PVDF is qualified as a polar semi-crystalline polymer with at least four crystalline forms, *i.e.* α-, β-, γ-, and δ-phases.[18] Among them, the α phase is the most common and stable polymorph due to the monoclinic unit cell with *trans–gauche–trans–gauche* chain conformation,[19] while β phase shows all-*trans* conformation comprising fluorine atoms and hydrogen atoms on opposite sides of the polymer backbone.[20] It is known that the peaks at 17.1°, 18.5° and 19.6° correspond to the α phase, while the peak at 20.6° corresponds to the β phase.[21] As can be seen from the XRD patterns of MA, MB and MC in Fig. 2, the predominant peak of the β phase of PVDF can be clearly observed in each membrane. For the α phase of PVDF, although very tiny, the most presentative peak of the α phase can still be detected from MB and MC when both patterns were compared with that of MA. The coexistence of both α and β phase is attributed to the similar atomic radii of hydrogen and fluorine atoms. With the poorest compatibility, the CC solution is representative of the lowest energy, which is beneficial for the formation of the most stable α phase in MC. As discussed in Section 2.1, the compatibility between the PVDF and the binary solvent is in the order of CC < CB < CA. Therefore, when phase separation occurs during the solidification process, a part of polymer chains in the α phase can obtain energy from the relatively high energy casting solution and transformed into the β phase in all-*trans* conformation, leading to the intensification of β phase in MB especially in MA.

Tensile strength is one of the crucial factors that influencing the industrial application of membranes.[22] The membrane vibration in membrane-aerated biofilm reactor system, the fluid tangential force on membrane in cross flow membrane distillation and other membrane processes had set rigorous requirements on the tensile strength of membranes.[23] The morphology, crystalline form and crystallinity degree of PVDF are recognized as three determinants of the tensile strength. Table 2 demonstrates the tensile strength of MA, MB and MC, the highest of which can be observed in MC. Firstly, the bicontinuous structure of MC homogeneously distributed the external force on the entire membrane, enhancing the mechanical property effectively.[24] Secondly, it is proved that the amount of stable α phase was very important in obtaining PVDF membrane with a higher tensile strength.[25] Therefore, the improvement of tensile strength was emphasized by the most

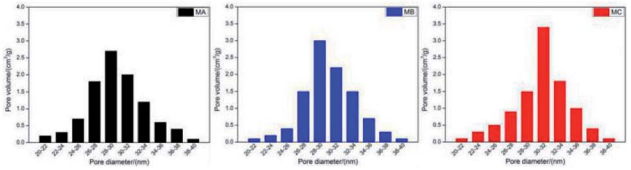

Fig. 3 The pore size distribution of membrane a (MA), membrane b (MB) and membrane c (MC) prepared from PVDF/GBL/DOP (casting solution a, CA), PVDF/GBL/DOA (casting solution b, CB), and PVDF/GBL/DOS (casting solution c, CC).

amount of α phase in MC. Thirdly, the much lower viscosity of DOS (19.9 mPa s) than DOP (81.4 mPa s) induced the higher mobility of PVDF chains during the crystallization at the same PVDF concentration, further improving the crystallinity degree mechanically of MC when compared with MA.[26] However, the slight difference of viscosity between DOS (19.9 mPa s) and DOA (13.7 mPa s) was not sufficient to produce a dramatic decrease on crystallinity degree between MC and MB. Due to the above mentioned aspects, the highest tensile strength at 6.37 MPa is obtained in MC. For MA and MB with the same cellular structure, crystalline form and crystallinity degree become the predominate factors in determining the tensile strength. On one hand, more α phase contained in MB is beneficial to the mechanical property. On the other hand, a much lower viscosity of DOA (13.7 mPa s) than DOP (81.4 mPa s) induced a higher mobility of PVDF chains and crystallinity degree of membrane. The more amount of α phase and the higher crystallinity degree induced the higher tensile strength of MB than MA. The best compatibility of CA also indicated the most entanglements and strongest physical interactions among the molecular chains of

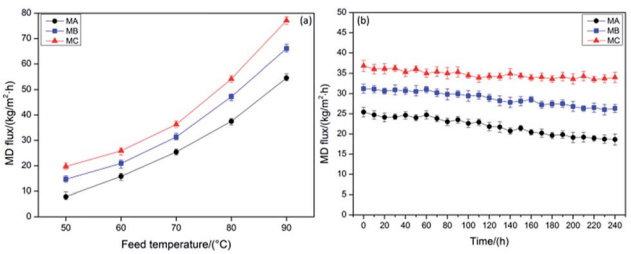

Fig. 4 The DCMD flux of membrane a (MA), membrane b (MB) and membrane c (MC) with (a) inlet feed temperatures from 50 to 90 °C when using 3.5 wt% NaCl solution as feed in a 24 h operation and with (b) prolonged time to 240 h at operation temperatures of 70 °C when using 3.5 wt% NaCl solution as feed.

Table 3 Performance comparison between the current work and the references

	Feed solution			Permeate solution				
Membrane	NaCl concentration (wt%)	Temperature (°C)	Flow rate (m s^{-1})	Temperature (°C)	Flow rate (m s^{-1})	Morphology	Permeate flux (kg m^{-2} h^{-1})	References
PVDF single-layer hollow fiber	3.5	81.3	1.80	17.5	1.20	A thin, sponge-like porous layer located between two thick layers full of finger-like macrovoids	79.2	34
PVDF single-layer hollow fiber	3.5	81.8	0.50	20	0.15	Long finger-like cavities, ultra-thin skin and the porous network sponge-like structure	40.5	35
PVDF/PTFE single-layer composite hollow fiber	3.5	80	1.94	17.5	0.95	A porous skin layer and a porous sponge-like substrate layer with finger-like macrovoids	40.4	36
PVDF single-layer hollow fiber	3.5	90	0.8	15.5	0.4	Lotus root-like morphology with seven uniformly distributed bore channels	69.1	37
PVDF@Cloisite15A single-layer hollow fiber	3.5	90	0.023	20	0.01	Large finger-like macrovoids stretched from the outer to the inner fiber skin	15.1	38
PVDF dual-layer hollow fiber	3.5	80	1.4	17	0.7	A macrovoid-free globular structure in the hydrophobic outer layer while the hydrophilic inner layer comprises a layer of macrovoids near the inner edge	83.4	39
PVDF dual-layer hollow fiber	3.5	90.3	1.60	16.5	0.80	Sponge like structure	37.4	40
PVDF dual-layer hollow fiber	3.5	78.2	1.8	16.6	0.72	The outer hydrophobic layer has a macrovoid-free structure, the inner hydrophilic layer has many macrovoids with irregular shapes	66.9	41
PVDF/PTFE dual-layer composite hollow fiber	3.5	80	1.90	17.5	0.90	Delamination-free and fully sponge-like structure	52.5	42
PVDF dual-layer hollow fiber	3	64.5	0.8	17	0.5	Macrovoids with different size and shape dominate the structure of the inner half annulus; whereas, the macrovoids with more uniform shape and the much smaller size existing in the outer half annulus of the fibers	21.0	43
PVDF/$CaCO_3$ composite hollow fiber	3.5	80.5	0.50	20.0	0.15	Three layers: a sponge-like porous layer located between two layers full of finger-like macrovoids	46.3	44
PVDF dual-layer hollow fiber	3.5	60	1.4	15	0.7	Dual-layer hollow fiber: a fully finger-like macrovoid inner-layer and a sponge-like outer-layer	98.6	45
PVDF/GO-NBA dual-layer hollow fiber	3.5	80	0.5	16	0.1	Dual-layer hollow fiber: a finger-like macrovoid inner-layer and a nodular structure outer-layer	61.9	46

Table 3 (*Contd.*)

Membrane	Feed solution: NaCl concentration (wt%)	Feed solution: Temperature (°C)	Feed solution: Flow rate (m s^{-1})	Permeate solution: Temperature (°C)	Permeate solution: Flow rate (m s^{-1})	Morphology	Permeate flux (kg m^{-2} h^{-1})	References
MA	3.5	90.0	0.80	25.0	0.80	Cellular structure with dense skin in the outer surface and macrovoids in the inner surface	56.1	This study
MB	3.5	90.0	0.80	25.0	0.80	Cellular structure with dense skin in the outer surface and macrovoids in the inner surface	68.5	This study
MC	3.5	90.0	0.80	25.0	0.80	Interconnected sponge-like structure with dense skin in the outer surface and macrovoids in the inner surface	77.6	This study

PVDF, leading to difficult slippage of chains under loading.[27] For this reason, MA exhibited the lowest elongation and could be qualified as the most vulnerable membrane of the three. In the same way, the compatibility of CB enabled a higher elongation of MB than that of MA and decreased the fragility of the membrane. The weakest compatibility of CC allowed a substantial increase in the free volume of PVDF molecules expansion under the external stress, thereby making MC the softest and most flexible of the three membranes. In general, the tensile strength of the membrane prepared by NIPS method is in the range of 2–4 MPa,[28] which is much lower than that of the membrane prepared by TIPS method in this study. By avoiding the formation of macrovoid and finger-like structure, the excellent mechanical property produced by TIPS approach shows a potential advantage in the industrial application.[29]

Table 2 and Fig. 3 delineate the porosity and pore size distribution of MA, MB and MC. The porosity of three membranes is in the range of 56.7–67.2% without dramatic difference due to the fixed PVDF concentration in the casting solution. The solvents in the casting solutions were extracted to be the pores while PVDF form the membrane skeleton after the extraction. In the L–L phase separation process of MA and MB, the polymer crystallized out of the polymer-rich phase droplets and initiated the spherulites.

Meanwhile the growing polymer-lean phase droplets are entrapped within the polymer spherulites with the decline of the temperature. The weaker compatibility of CB caused the longer coarsening time of polymer-lean phase droplets, further leading to the pores with more uniform size connecting the cells in the cellular structures.

In the L–L phase separation process of MC, the polymer-rich phase droplets in this casting solution transferred into the spherulites with interconnected pores when the temperature decreased. At the same time, the boundary among the polymer-lean phase droplets disappeared and gap junction pores are originated gradually during their collision. The largest gap between the binodal curve and crystallization curve induced the enough time for the growth and connection of interconnected pores and gap junction pores. Therefore, the biggest pore size and narrowest pore size distribution of bicontinuous structure are derived in MC.

3.2. Performance in DCMD process

The DCMD flux of MA, MB and MC varied with inlet feed temperatures from 50 to 90 °C when using 3.5 wt% NaCl solution as feed in a 24 h operation is shown in Fig. 4a. No obvious change in the membrane thickness was listed in Table 2, revealing the stable membrane size throughout the entire fabrication process and normalizing the effect of thickness on DCMD performance. It also can be observed that the DCMD flux of MB is higher than MA, which is accordance with the more uniform pore size of MB aforementioned. According to the biggest pore size and narrowest pore size distribution discussed above, MC indicated a highest DCMD flux when compared with MA and MB at the same temperature. Intrinsically, the high connectivity of bicontinuous structure in MC was seemed to be another decisive factor for higher permeability than the other two membranes. The DCMD flux of MC achieved 77.5 kg (m^2 $h)^{-1}$ at the feed temperature of 90 °C, which reached the international advanced level.[30,31] The detected solution conductivity of the distillate was less than 40 μS cm^{-1}, which demonstrated that the NaCl rejection rate of three membranes was above 99.99%.

Table 3 lists a performance comparison in DCMD process between the current work and the references. The DCMD flux of MC reached 77.6 kg (m^2 $h)^{-1}$ at the feed temperature of 90 °C, illustrating the self-fabricated PVDF hollow fiber membranes in this work have comparable or even better performance than the membranes reported in the ref. 32–44.

The long-term DCMD operations for MA, MB and MC were conducted within 240 h at operation temperatures of 70 °C when using 3.5 wt% NaCl solution as feed, and the variations in flux were illustrated in Fig. 4b. There is an 18.34% decrease in MC over the 240 h of the operation, which is much lower than

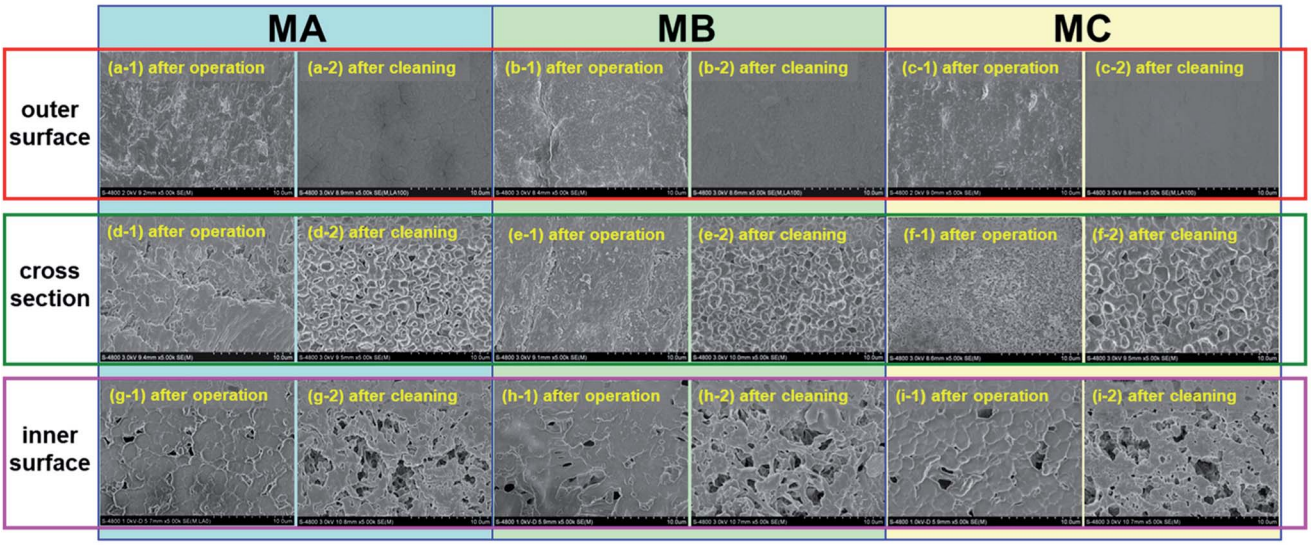

Fig. 5 The morphology of the outer surface (a–c), cross section (d–f), and inner surface (g–i) of membranes MA (left two columns), MB (middle two columns), and MC (right two columns) after a 240 h operation (no. 1 on the left of the two columns for each membrane) and after a chemical cleaning process (no. 2 on the right of the two columns for each membrane).

that of MA (29.47%) and MB (23.08%). As the system proceeded, NaCl in the feed would be saturated or oversaturated, and thus began to crystallize on the surface of the membranes due to the effect of concentration polarization. Besides, the contaminants which have been presented in the feed solution and dust which has entered in MD system during the operation may deposited on the membrane surface and accumulated inside the pores, although no foulants were added to the feed solution.[45–48] Fig. 5 illustrates the morphology of the membrane before (after operation) and after chemical cleaning. From the images shown in Fig. 5, a fouling layer was completely formed and fully covered on the outer and inner surfaces of all membranes after operation. And simultaneously, the pores of the membrane were partially or completely blocked from the microstructures of the cross section. However, from the membrane morphology after chemical cleaning, it can be clearly observed that most of the foulants were removed and the pores reappear in the cross section. There is no obvious difference between the morphology of the original membranes (Fig. 1) and the cleaned membranes, which indicates that the membrane structure has not been changed under the DCMD operating conditions. The membrane fouling reduced the temperature difference across the membrane, which is likely to contribute to both thermal and hydraulic resistances, and thereby caused the less driving force. Therefore, a flux decrease with time over the 240 h of continuous operation in each membrane can be observed, even if the flux can be very stable for the first 50 h. The initial MD flux and flux decline pattern were in the order of MC > MB > MA, revealing more excellent long-term performance of MC.

4. Conclusions

In this work, different membrane structures for the direct contact membrane distillation (DCMD) process were discussed in terms of phase diagram analysis, binary solvent determination, membrane properties and performance comparison. Butyrolactones (GBL)/dioctyl-phthalate (DOP) and GBL/dioctyl adipate (DOA) binary solvents were employed to generate porous PVDF hollow fiber membranes with cellular structure, while the bicontinuous structure was produced from GBL/dioctyl sebacate (DOS) binary solvent by the thermally induced phase separation (TIPS) approach. The phase diagram was introduced to explain feasible formation mechanisms of the different structures. The morphology and properties of the hollow fiber membranes were characterized and compared. The membrane with a bicontinuous structure exhibited the largest amount of the α phase, the highest tensile strength, the most uniform pore size distribution, the highest DCMD flux and the best long-term performance when compared with the other two membranes with a cellular structure. The tensile strength of the membrane with a bicontinuous structure reached 6.37 MPa, and the DCMD flux achieved was 77.5 kg $(m^2\ h)^{-1}$ at a feed temperature of 90 °C, indicating the potential prospect of membranes with a bicontinuous structure in the membrane distillation (MD) process.

Conflicts of interest

There are no conflicts to declare.

Acknowledgements

The authors gratefully acknowledge Shenzhen Science and Technology Innovation Committee (Grant No. GRCK2017042411043692, JCYJ20160429191618506), the Science and Technology Project of Tianjin China (Grant No. 12ZCZDSF02200) and the National Key Technology R&D Program of China (Grant No. 2006BAB03A06).

References

1 Z. Song, M. Xing, J. Zhang, B. Li and S. Wang, *Sep. Purif. Technol.*, 2012, **90**, 221.
2 R. Moradi, J. Karimi-Sabet, M. Shariaty-Niassar and Y. Amini, *Chem. Eng. Process.*, 2016, **100**, 26.
3 D. Zhao, J. Zuo, K. J. Lu and T. S. Chung, *Desalination*, 2017, **413**, 119.
4 O. R. Lokare, S. Tavakkoli, G. Rodriguez, V. Khanna and R. D. Vidic, *Desalination*, 2017, **413**, 144.
5 F. Vigo, C. Uliana, B. Cavazza and F. Salvemini, *J. Membr. Sci.*, 1984, **21**, 295.
6 D. Y. Hou, J. Wang, D. Qu, Z. K. Luan and X. J. Ren, *Sep. Purif. Technol.*, 2009, **69**, 78.
7 M. Mulder, *Basic principles of membrane technology*, Kluwer Academic, The Netherlands, 1996, p. 71.
8 Z. Song, W. Yang, J. Zhang, Y. Li and S. Yuan, *J. Polym. Eng.*, 2015, **35**, 709.
9 Y. Tang, Y. Lin, W. Ma, Y. Tian, J. Yang and X. Wang, *J. Appl. Polym. Sci.*, 2010, **118**, 3518.
10 Q. Zhou, Z. Wang, H. Shen, Z. Zhu, L. Liu, L. Yang and L. Cheng, *J. Chem. Technol. Biotechnol.*, 2016, **91**, 1697.
11 Q. Zhou, Z. Wang, H. Shen, Z. Zhu, L. Liu, L. Yang and L. Cheng, *J. Chem. Technol. Biotechnol.*, 2016, **91**, 1697.
12 J. Yang, D. Li, Y. Lin, X. L. Wang, F. Tian and Z. Wang, *J. Appl. Polym. Sci.*, 2008, **110**, 341.
13 Y. H. Tang, Y. D. He and X. L. Wang, *J. Membr. Sci.*, 2012, **409**, 164.
14 B. S. Lalia, V. Kochkodan, R. Hashaikeh and N. Hilal, *Desalination*, 2013, **326**, 77.
15 R. C. Weast, M. J. Astle, and W. H. Beyer, *CRC handbook of chemistry and physics*, CRC press, Boca Raton, FL, 1988.
16 J. Su, T. S. Chung, B. J. Helmer and J. S. de Wit, *J. Membr. Sci.*, 2012, **396**, 92.
17 T. Ishigami, K. Nakatsuka, Y. Ohmukai, E. Kamio, T. Maruyama and H. Matsuyama, *J. Membr. Sci.*, 2013, **438**, 77.
18 A. J. Lovinger and I. D. C. Basset, *Developments in Crystalline Polymers*, Elsevier Applied Science, London, 1st edn, 1982.
19 A. S. ELmezayyen, F. M. Reicha, I. M. El-Sherbiny, J. Zheng and C. Xu, *Eur. Polym. J.*, 2017, **90**, 195.
20 V. Sencadas, R. Gregorio Jr and S. Lanceros-Méndez, *J. Macromol. Sci., Part B: Phys.*, 2009, **48**, 514.
21 G. T. Davis, J. E. McKinney, M. G. Broadhurst and S. Roth, *J. Appl. Phys.*, 1978, **49**, 4998.
22 J. Mulder, *Basic principles of membrane technology*, Springer Science & Business Media, 2012.
23 Z. Karim, S. Claudpierre, M. Grahn, K. Oksman and A. P. Mathew, *J. Membr. Sci.*, 2016, **514**, 418.
24 Z. Wang, L. Sun, Q. Wang, B. Li and S. Wang, *Eur. Polym. J.*, 2014, **60**, 262.
25 M. G. Buonomenna, P. Macchi, M. Davoli and E. Drioli, *Eur. Polym. J.*, 2007, **43**, 1557.
26 M. M. Nasef, H. Saidi, H. M. Nor and O. M. Foo, *J. Appl. Polym. Sci.*, 2000, **78**, 2443.
27 S. L. Shenoy, W. D. Bates, H. L. Frisch and G. E. Wnek, *Polymer*, 2005, **46**, 3372.
28 F. Liu, N. A. Hashim, Y. Liu, M. R. M. Abed and K. Li, *J. Membr. Sci.*, 2011, **375**, 1.
29 G. Kang and Y. Cao, *J. Membr. Sci.*, 2014, **463**, 145.
30 S. Bonyadi and T. S. Chung, *J. Membr. Sci.*, 2009, **331**, 66.
31 Y. Tang, N. Li, A. Liu, S. Ding, C. Yi and H. Liu, *Desalination*, 2012, **287**, 326.
32 K. Y. Wang, S. W. Foo and T. S. Chung, *Ind. Eng. Chem. Res.*, 2009, **48**, 4474.
33 D. Y. Hou, J. Wang and D. Qu, *Sep. Purif. Technol.*, 2009, **69**, 78.
34 M. M. Teoh and T. S. Chung, *Sep. Purif. Technol.*, 2009, **66**, 229.
35 P. Wang and T. S. Chung, *J. Membr. Sci.*, 2012, **421**, 361.
36 N. M. Mokhtar, W. J. Lau, A. F. Ismail and B. C. Ng, *RSC Adv.*, 2014, **4**, 63367.
37 F. Edwie, M. M. Teoh and T. S. Chung, *Chem. Eng. Sci.*, 2012, **68**, 567.
38 S. Bonyadi and T. S. Chung, *J. Membr. Sci.*, 2007, **306**, 134.
39 M. Su, M. M. Teoh, K. Y. Wang, J. Su and T. S. Chung, *J. Membr. Sci.*, 2010, **364**, 278.
40 M. M. Teoh, T. S. Chung and Y. S. Yeo, *Chem. Eng. J.*, 2011, **171**, 684.
41 Z. W. Song and L. Y. Jiang, *Chem. Eng. Sci.*, 2013, **101**, 130.
42 D. Y. Hou, J. Wang, X. C. Sun, Z. G. Ji and Z. K. Luan, *J. Membr. Sci.*, 2012, **405**, 185.
43 P. Wang, M. M. Teoh and T. S. Chung, *Water Res.*, 2011, **45**, 5489.
44 K. J. Lu, J. Zuo and T. S. Chung, *J. Membr. Sci.*, 2017, **539**, 34.
45 T. V. Knyazkova and A. A. Maynarovich, *Desalination*, 1999, **126**, 163.
46 H. Zhu and M. Nyström, *Colloids Surf., A*, 1998, **138**, 309.
47 E. M. V. Hoek, J. Allred, T. Knoell and B. H. Jeong, *J. Membr. Sci.*, 2008, **314**, 33.
48 M. Gryta, *J. Membr. Sci.*, 2008, **325**, 383.